Journal of Thermal Analysis and Calorimetry, Vol. 63 (2001) 397–413

DSC EVALUATIONS IN F.C.C. SOLID SOLUTIONS OF SHORT-RANGE-ORDER KINETICS AS INFLUENCED BY BOUND VACANCIES

A. Varschavsky and E. Donoso

Universidad de Chile, Facultad de Ciencias Físicas y Matemáticas, Instituto de Investigaciones y Ensayes de Materiales, IDIEM, Casilla 1420, Santiago, Chile

(Received August 8, 2000)

Abstract

A modified first order kinetic law, which describes the roles of bound and unbound vacancies, is proposed in order to predict defect decay and short-range-order kinetics of quenched binary alloys during linear heating experiments. The model has been applied to differential scanning calorimetry (DSC) curves of Cu–5 at%Zn quenched from different temperatures. Activation energy for migration of solute-vacancy complexes was also assessed from the kinetics of short-range-order using DSC traces. A value of 89.5±0.32 kJ mol^{-1} was obtained. The relative contribution of bound and unbound vacancies to the ordering process as influenced by quenching temperature was determined. In conjunction, a parametric study of the initial total defect concentration and effective energy for defect migration was performed in order to envisage their influence on the calculated DSC profiles.

Keywords: Cu–5 at%Zn, DSC, F.C.C. (Face Centered Cubic), kinetics, short-range-order, solute-vacancy complexes

Introduction

Different characteristics of short-range-order (SRO) in f.c.c. solid solutions have been studied for a long time by diffuse scattering of X-rays [1–6], by small-angle X-ray scattering [7], by electron microscopy and electron diffraction [8–12], by determination of elastic and plastic properties [13–15] and strengthening and fatigue properties [16–21], as well as by electrical resistivity [22–25] and thermal analysis [13, 14, 18, 26–31].

Contrary to usual experiments on SRO kinetics after quenching from rather high temperatures, some experiments are focused on the adjustment of the new equilibrium state of SRO established after small and sudden temperature changes [32–36] and others are now related with the influence of cold work [37–40]. Nevertheless, quenching experiments still provide information about how excess vacancies frozen during the quench can affect the alloy ordering kinetics [41–45]. For instance, differential scanning calorimetry (DSC) of thermally disordered alloys reveals that short-range-ordering generally takes

1418–2874/2001/ $ 5.00

Akadémiai Kiadó, Budapest
Kluwer Academic Publishers, Dordrecht

place in two stages, irrespective of the alloy system: stage-1, ordering at low temperatures is associated with the migration of excess defects, and stage-2, ordering at higher temperatures is due to the migration of equilibrium defects. It is worth noticing that in some cases ordering is associated only with stage-1, as in the present study. The features revealed by the DSC traces have been explained quantitatively [43], predicting the relative importance of each stage. Therefore, information was gained on the ordering process itself and vacancy behaviour.

While solid solution alloy systems exhibiting SRO are rather extensively investigated [46], there are only few investigations of the role of solute-vacancy complexes [47], which are determinant in explaining important features of several metallurgical processes [48–52]. It is then important to examine the role of such complexes in the ordering process, to the end of giving an account of the observed behaviour of the differential scanning calorimetry traces displayed after specific experiments, in which they are present.

Chiefly, the present work: (a) designs experiments which provide evidence of solute-vacancy complexes in a one-stage ordering process (b) discloses a model that predicts the return of unbound and bound vacancies to equilibrium, describing also the kinetics of reordering (c) tests its validity for Cu–5 at%Zn, (d) from this model activation energy for migration of bound vacancies can be assessed using DSC data and (e) performs a parametric study of the initial total defect concentration and effective activation energy for defect migration in order to establish their influence on calculated DSC profiles.

Theoretical considerations

Freezing defect concentration after quenching

Firstly it is worth pointing out in this section that during quenching, unbound and bound vacancies can migrate because the cooling rate is finite in practical experiments. Above the freezing temperature T_z, the reactions between the defects are considered to be in the thermal dynamical equilibrium because they are fast enough to maintain it between them during quenching from temperature T_q, as profusely reported [53–57]. Even if bound vacancies become less mobile dynamic equilibrium exists assisted only by the association/dissociation mechanism.

One of the aims of this section is to assess the relative concentration of bound vacancies after quenching and also to investigate their redistribution at the beginning of a DSC run after small transient periods have elapsed [53–57].

In fact, for moderate diluted alloys, we will be dealing with in the present work [58]:

$$\frac{c_b}{c_u} = \frac{Zx_t \exp\left(\frac{B}{RT}\right)}{1-(Z+1)x_t + Zx_t \exp\left(\frac{B}{RT}\right)} \tag{1}$$

where c_u and c_b are the unbound and bound vacancy concentrations, Z is the coordination number, x_t is the solute concentration and B is the solute-vacancy binding energy. Thus, in c_t is the total defect concentration, one has:

$$\frac{c_b}{c_t} = \frac{Zx_t \exp\left(\frac{B}{RT}\right)}{1-(Z+1)x_t + 2Zx_t \exp\left(\frac{B}{RT}\right)} = \psi_b(T) \tag{2}$$

and

$$\frac{c_b}{c_t} = \frac{1-(Z+1)x_t + Zx_t \exp\left(\frac{B}{RT}\right)}{1-(Z+1)x_t + 2Zx_t \exp\left(\frac{B}{RT}\right)} = 1-\psi_b(T) \tag{3}$$

where $\psi_b(T)$ is here termed the equilibrium transfer function.

As dynamical equilibrium exists during quenching [53–57], the concentrations $c_b(T_z)$ and $c_u(T_z)$ at the freezing temperature can be readily calculated from:

$$c_b(T_z) = c_t(T_z)\psi_b(T_z) \tag{4}$$

and

$$c_u(T_z) = c_t(T_z)(1-\psi_b(T_z)) \tag{5}$$

The freezing temperature T_z can be estimated from [43]

$$\frac{E_m}{RT_z'} = \ln\left(\frac{RT_{z2}}{\phi_q \tau_0 E_m}\right) \tag{6}$$

where $\tau_0=10^{-6}$ s [43] and ϕ_q is the cooling rate. It should be pointed out that the more mobile unbound vacancies with migration energy E_m determine T_z. Since for this alloy concentration c_b is close to c_u, separating from each other somewhat with increasing temperature [58], it is safe to take as a first approximation and average activation energy for defect formation and hence.

$$c(T_z) = A_s \exp\left(-\frac{E_{ef}}{RT_z}\right) \tag{7}$$

where $E_{ef}=E_f-B/2$ and $A_s\approx 2$ [43].

Unbound and bound vacancy redistribution after de-freezing

At the de-freezing temperature T_i, where the same ordering condition as that at T_z (the freezing temperature) prevails, a short transient period begins in which a redistribution of unbound and bound vacancies takes place. It is assumed that at temperature T_c,

the measured extrapolated peak onset temperature, these short transient effects just vanish but the total defect concentration still remains the same as at T_z, T_i and T_e [53, 54]. After redistribution of unbound and bound vacancies have taken place a pseudo-equilibrium state is established between them [53, 54]; all defects decay to a negligible value at a rate governed by their kinetic path when the final trace temperature is reached at T_f (all these temperatures are illustrated in Fig. 1), since we will be concerned in this work with one stage ordering assisted by excess defects. That is, true equilibrium is reached at T_f where also equilibrium concentration of thermal defects can be disregarded. It is worth noticing that the term pseudo-equilibrium was also employed here as in other works [53–55], because if the run is interrupted at certain arbitrary temperature between T_e and T_f, the instantaneous defects concentration decrease isothermally to zero with time along the corresponding kinetic path in equilibrium between them. This concept is different to dynamic equilibrium, which is a true equilibrium state taking place while changing temperature.

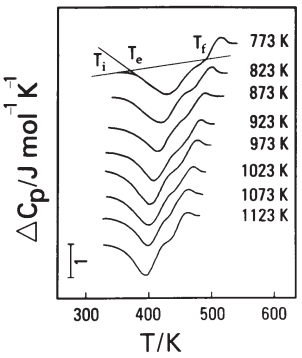

Fig. 1 DSC curves for Cu-5 at% Zn quenched from the indicated temperatures. ϕ_r=0.33 K s^{-1}. Initial (T_i), extrapolated onset (T_e), and final (T_f) temperatures are indicated

As said before, it was assumed that one criterion for determining the transient range temperature is to measure the temperature interval $\Delta T=T_e-T_i$, since it is not possible to assess its temperature range with higher accuracy. However, it is reasonable to assume that the larger the defect redistribution is the larger the interval ΔT is. In general calorimetric methods are not able to detect heat effects taking place during these short transients at constant total defect concentration, as resistivity measurements are. Furthermore, it is worth noticing that one indication that transients would take place between T_i and T_e is that $(T_i-T_e)/\phi_r>t_t$, being ϕ_r the heating rate and t_t the transient time period. It is likely that this unequality actually remains under our experimental conditions, since $t_t\approx 8$ s on an isothermal annealing at 453 K [55]. Therefore, the pseudo-equilibrium concentration of defects after this transient period can be stated in a first approximation as:

$$C_t(T_z) = c_t(T_i) = c_t(T_e) \tag{8}$$

$$c_b(T_e) = c_t(T_z)\psi_b(T_e) \quad (9)$$

$$c_u(T_e) = c_t(T_z)(1-\psi_b(T_e)) \quad (10)$$

Notice that the assumption $c_t(T_z) = c_t(T_i) = c_t(T_e)$ stated above is used. That is, the total defect concentration before transient was in principle the same as the one, which exists immediately after the transient behaviour, vanishes [53, 55]. However, c_u and c_b redistribute each other during the temperature interval ΔT.

Effective rate constant for SRO

The effective activation energy for defect migration is a weightened average value between those of unbound and bound vacancies, that is:

$$E = (1-\alpha)E_m+\alpha E_c \quad (11)$$

where E_c is the activation energy for migration of solute-vacancy complexes and α is a strengthening factor. If, theoretically, all defect transport would occur by bound vacancies, which is not the case [59], α=1, on the contrary for unbound vacancy transport only, α=0. The value of α is constant along the DSC run if E also is. Besides, it is worth noticing that E_c is a mean quantity since it is well known that the mobility of solute-vacancy pairs depends on the frequency of vacancy jumps around the solute atom, as well as on the frequency of solute-vacancy exchanges. Therefore, there is not a unique activation energy.

The effective rate at which order is established for a point defect mechanism, which is supposed to include bound and unbound vacancies, is related to the total instantaneous defect concentration c_t, and to the effective mean rate at which defect atom exchange occurs, that is by

$$k_t(T) = c_t(T)\nu_t(T) \quad (12)$$

in which

$$\nu_t(T)=\nu_{ot}\exp\left(-\frac{R}{RT}\right) \quad (13)$$

ν_{ot} being the effective jump frequency constant, T the absolute temperature, and R the universal gas constant. Here it will be considered that $c_t = c_u+c_b$ with c_u and c_b equal to the unbound and bound vacancy concentrations. Now, for simultaneous unbound and bound vacancy mechanisms the effective rate constant can be stated as:

$$k_t = \nu_u c_u+\nu_b c_b \quad (14)$$

where ν_u and ν_b are the jump frequencies of unbound and bound vacancies, that is [60]:

$$\nu_t(c_u+c_b) = \nu_u c_u+\nu_b c_b \quad (15)$$

The idea contained in Eq. (15) is that the entire population of vacancies, unbound and bound, is assigned one effective jump frequency, ν_t, which is obtained as a weightened sum of simpler jump frequencies describing individual processes. From Eqs (2), (3) and (15) one has:

$$\nu_t = \nu_u(1-\psi_b(T))+\nu_b\psi_b(T) \tag{16}$$

The simplier jump frequencies are given by:

$$\nu_u = \nu_{om}\exp\left(-\frac{E_m}{RT}\right) \tag{17}$$

and

$$\nu_b = \nu_{om}\exp\left(-\frac{E_c}{RT}\right) \tag{18}$$

The attempt frequency ν_{om} is considered to be the same for unbound and bound vacancies [60]. Therefore, the effective attempt frequency can be safely taken also as $\nu_{om}=12\nu_0\exp(\Delta S_m/R)$ for f.c.c. alloys, where ν_0 is the Debye frequency and ΔS_m the activation entropy for free vacancies [45].

Effective defect decay and short-range ordering kinetics

Here we consider that sink strengths of bound and unbound vacancies are the same and the total vacancy supersaturation follows a first order kinetic path, as expected from its elimination at fixed sinks [61]. It is also assumed that at the end of the DSC trace at T_f, equilibrium is attained and the total defect concentration $c_t^{eq}=0$ since $c_t(T_z)>> c_t^{eq}(T_f)$, as long as we are concerned with one stage ordering process. Furthermore, the present analysis implies solute-vacancy complexes production and dissolution during the run, since the above-mentioned state of pseudo-equilibrium prevails in the alloy during the heating process. Using the effective vacancy jump frequency ν_t, defect supersaturation, formally defined as $S=(c_t(T)-c_t^{eq})/(c_t(T_z)-c_t^{eq})$, decays according to:

$$\frac{dS}{dT}=-\frac{k_d S}{\phi_r} \tag{19}$$

where ϕ_r is the heating rate and $k_d=\nu_t\rho_t$, the rate constant which is of Arrhenius type, ρ_t is the effective sink density. ρ_t is given by:

$$\rho_t = \rho_d+\rho_g \tag{20}$$

where ρ_d, the sink density for dislocations can be obtained from:

$$\rho_d=\frac{2\pi b^2\delta}{\ln\left(\frac{r_s}{r_c}\right)} \tag{21}$$

being r_s equal to the average distance between dislocations, r_c the capture radius of a dislocation, δ the dislocation density and b the atom jump distance. For grain boundaries, the sink density ρ_g is given by:

$$\rho_g = \frac{\lambda}{L^2} \tag{22}$$

where $\lambda = a_0^2/12$ for f.c.c. metals, a_0 is the lattice parameter and L the grain size. Using the definition of S given before and considering roughly as a first approximation that $c_t^{eq} = 0$, integration of Eq. (19) yields:

$$c_t(T) = c(T_z)\exp\left[-\frac{\rho_d + \rho_g}{\phi_r}\int_0^T \nu_{0m}\exp\left(-\frac{E}{RT}\right)dT\right] \tag{23}$$

or:

$$c_t(T) = c_t(T_z)\exp[-(\rho_d+\rho_g)\nu_{0m}\theta(E,T)] \tag{24}$$

where θ, the reduced time, is given by [62–64]:

$$\theta(E,T) = \frac{RT^2}{\phi_r E}\exp\left(-\frac{E}{RT}\right) \tag{25}$$

Furthermore, it has been demonstrated [47] that the formation of solute-vacancy pairs occurs on the quick time scale for vacancy relaxations, and for most purposes the number of such pairs can be assumed to be in equilibrium with the state of chemical order in the alloy.

From the above analysis it is inferred that defect decay concentrations should permanently adjust through the transfer function $\psi_b(T)$ to maintain pseudo-equilibrium between them along the DSC run. Henceforth, its decay kinetics follows the relationship:

$$c_b(T) = c_t(T)\psi_b(T) \tag{26}$$

and

$$c_u(T) = c_t(T)[1-\psi_b(T)] \tag{27}$$

It should be kept in mind that these equations and also Eq. (24) give approximate determinations, since in their derivation the composite quantity ν_t is involved, which is an effective jump frequency. Decay defect curves will be shown later on in a section concerning numerical results for different quenching temperatures, previous determination of the effective activation energy E as will be assessed from non-isothermal short-range ordering kinetic analysis.

As long as the ordering process can be described by a first-order like kinetic law, as can be done for most binary alloy systems [65], the differential equation for the transformed fraction y under a linear heating becomes:

$$\frac{dy}{dT}=\frac{k_t}{\phi_r}(1-y) \tag{28}$$

where $k_t = \nu_t c_t$ is the rate constant. Unlike k_d, constant k_t is not of Arrhenius type. Integration of Eq. (28) yields:

$$y=1-\exp\left[-\frac{1}{\phi_r}\int_0^T k_t dT\right] \tag{29}$$

From Eqs (13), (24) and (25) after some modifications, Eq. (29) can be written as:

$$y=1-\exp\left[-\frac{c_t(T_z)}{\phi_r(\rho_d+\rho_g)}\int_0^T F_E(T)dT\right] \tag{30}$$

where the function $F_E(T)$ is given by:

$$F_E(T)=k_d\exp\left(-k_d\frac{RT^2}{\phi_r E}\right) \tag{31}$$

Adjustment of Eq. (30) to each experimental *y vs. T* curve can be made numerically with *E* as a disposable parameter. Thus, the best fit allows to determine the effective activation energy for defect migration based on a distributed function along the DSC temperature interval. Once *E* is determined for each quenching temperature calculated bound, unbound and total vacancy concentration curves can be plotted against temperature scanned in DSC traces.

An activation energy value for migration of vacancy-solute complexes can be assessed from:

$$y=1-\exp\left[-\frac{\nu_{om}c_t(T_z)}{\phi_r}\int_0^T F_c(T)dT\right] \tag{32}$$

where the function F_c is given by:

$$F_c(T)=\beta\exp\left[-\frac{(\rho_d+\rho_g)\nu_{0m}T\beta}{\phi_r\ln\left(\frac{1}{\beta}\right)}\right] \tag{33}$$

in which,

$$\beta=\exp\left(-\frac{E_c}{RT}\right)\psi_b(T)+\exp\left(-\frac{E_m}{RT}\right)[1-\psi_b(T)] \tag{34}$$

Numerical adjustment of Eq. (32) to each experimental curve with E_c as a disposable parameter gives activation energies for solute-vacancy complexes. As it will

be seen later on, such values approach an average one which is essentially insensitive to the quenching temperature.

In the following, we will evaluate – by means of DSC – ordering kinetics and defect decay concentrations in a high rate quenched copper–zinc solid solution from different temperatures where equilibrium SRO is reached in one stage during a DSC experiment.

Numerical application concerning Cu–5 at%Zn

The alloy studied contained 5.1 mass% zinc (99.97 mass%). It was prepared in a Baltzer VSG 10 vacuum induction furnace from electrolytic copper (99.95 mass%) in a graphite crucible. The ingot was subsequently forged at 923 K to a thickness of 10 mm, pickled with a solution of nitric acid (15% in distilled water) to remove surface oxide, annealed in a vacuum furnace at 1123 K for 36 h to achieve complete homogeneity, and cooled in the furnace to room temperature. It was then cold-rolled to a thickness of 1.5 mm with intermediate annealing periods at 923 K for 1 h. After the last anneal, the material was finally rolled to a thickness of 0.75 mm (50% reduction).

Subsequent heat treatments were performed at different temperatures for 1 h, followed by quenching in a high rate quenching device developed in our laboratory. The quench time was measured with an oscilloscope and estimated in 200 ms. Such high quench rates were used in order to promote a one stage ordering process via an excess of unbound and bound vacancies from all selected quenching temperatures. That is, by minimizing defect losses during the quench, sufficient defects in excess are available to reach an equilibrium state of short-range-order. Otherwise, reordering involves two stage processes, the first assisted by excess defects and the second by equilibrium defects [41, 42]. A one-stage process facilitates to visualize the roles of unbound and bound vacancies.

Microcalorimetric analysis of the samples was performed in a DuPont 2000 thermal analyzer. Specimen discs 0.75 mm in thickness and 6 mm in diameter were prepared. Differential scanning calorimetric measurements of the heat flow were made by operating the calorimeter in the constant heating rate mode. Runs were made from room temperature to 740 K. To increase the sensitivity of the measurements, a high purity, well-annealed copper disc, in which no thermal events occur over the range of temperatures scanned, was used as a reference. In order to minimize oxidation, dried nitrogen ($0.8 \cdot 10^{-4}$ m^3 min^{-1}) was passed through the calorimeter. The baseline was determined in the following way. After each test, the data were converted to a differential-heat-capacity *vs*. temperature using a previously established calibration for the DSC cell. Subsequently a linear baseline was subtracted from the data. This baseline represents the temperature dependent heat capacity of the Cu–Zn solid solution in the existing thermal condition and its value was in agreement with the Kopp–Newmann rule. Heat capacity remainder, namely ΔC_p represents the heat associated with the solid-state reactions that take place during the DSC run.

DSC measurements and the role of solute-vacancy complexes in the ordering process

Typical DSC curves for the alloy under study at the indicated quenching temperatures are shown in the differential heat capacity ΔC_p *vs*. temperature T curves at a heating rate ϕ_r=0.33 K s^{-1} in Fig. 1. The initial temperature T_i, the extrapolated onset post-transient temperature T_e and the final temperature T_f are indicated in the curve corresponding to the quenching temperature of 773 K. In all cases they are characterized by one exothermic peak, namely stage 1 and one endothermic peak, stage 2. Stage 1 has been reported in the literature in connection with short-range order development assisted by excess defects, while stage 2 has been associated with a disordering process [44, 45]. It can be observed that in the present type of experiments (high quench rates), all stages shift to higher temperatures as the quenching temperature decreases. Stage 1 and 2 shifting will be associated with the relative increased contribution of solute-vacancy complexes as quenching temperature is lowered. The enthalpimetric features of these curves will be considered in a later work as they are not directly involved with the scope of the models developed here.

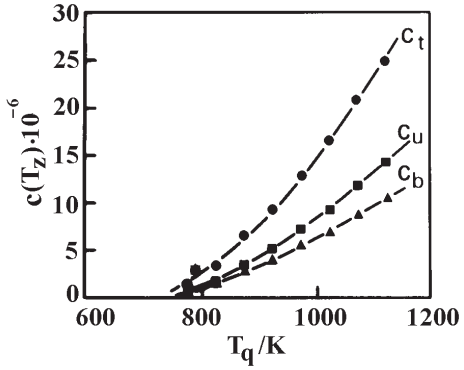

Fig. 2 Bound (c_b), unbound (c_u) and total vacancy concentration (c_t) at freezing temperature as a function of quenching temperature

The contribution of bound and unbound vacancy concentrations before peak initiation can be readily computed by means of Eqs (4) and (5), utilizing the equilibrium transfer function $\psi_b(T_z)$ at freezing temperature T_z calculated from Eq. (6), after estimation of $c_t(T_z)$ from Eq. (7). The value of solute-vacancy binding energy was taken as B = 21.8 kJ mol^{-1} [44]. Cooling rates were calculated from $\phi_q = (T_q - T_0)/t_q$, where the quench-in temperature was T_0= 273 K. A quench time t_q= 200 ms was estimated as stated earlier. These quenched-in defect concentrations $c_t(T_z)$, $c_u(T_z)$ and $c_b(T_z)$ as a function of the quenching temperature are shown in Fig. 2. It can be observed that the relative importance of c_b with respect to c_u increases as the quenching temperature is decreased and that all defect concentrations are decreased when this temperature also is, as expected. The relative importance of bound vacancies involved at the beginning of the ordering process described by $(c_b/c_u)T_e$ increase as the ratio $(c_b/c_u)T_z$ also does,

that is, when T_q is decreased as shown in Fig. 3. These results are also in agreement with the observed increase in effective activation energies and peak temperatures when T_q is lower as shown later on.

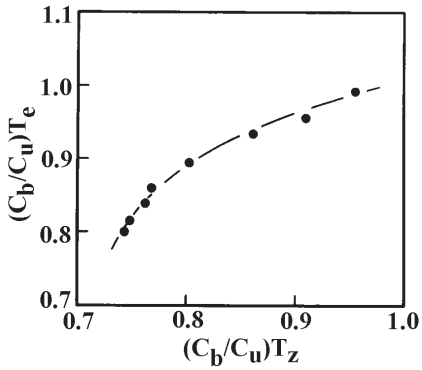

Fig. 3 Ratio of bound to unbound vacancy concentration at T_e *vs*. the same ratio at T_z

The influence of quenching temperature on the transient temperature interval, after de-freezing at the beginning of DSC runs will be briefly discussed. This can be done with reference to Fig. 4. In this figure the ratio of bound to unbound vacancies at the freezing temperature is plotted *vs*. the temperature interval $\Delta T = T_e - T_i$. If quenching temperature increases, T_z value also does so while $(c_b/c_u)T_z$ decrease (Fig. 2); its value becoming further away from pseudo-equilibrium value which would be established at T_e. Hence, in order to accomplish with such pseudo-equilibrium state a larger defect redistribution and consequently a larger temperature interval is required. On the contrary, if T_q and then T_z are lower, $(c_b/c_u)T_z$ increases and the defect ratio is closer to that required at T_e, hence a shorter temperature interval is needed to display the transient period.

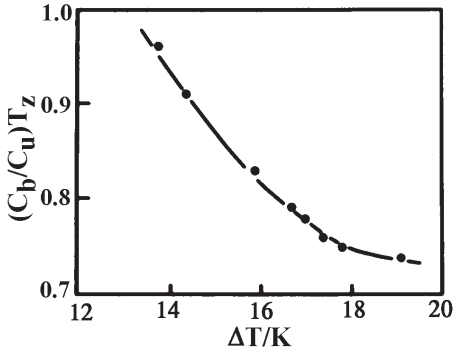

Fig. 4 Ratio of bound to unbound vacancy concentration at T_z *vs*. the transient temperature interval ΔT

Ordering kinetics and defect annihilation

Before computing short-range-order kinetics and defect decay curves according to Eqs (30), (32) and (24) sink density for dislocations and grain boundaries must be estimated together with other alloy parameters. For a typical annealed material the dislocation density is $\delta = 10^7$ cm^{-2} [43]. For this value the term $2\pi b^2/\ln(r_s/r_c)$ or Eq. (21), which is relatively insensitive to the dislocation density for annealed alloys was $4.4\cdot10^{-16}$ cm^2 and hence $\rho_d = 4.4\cdot10^{-9}$. The measured grain size was $L = 100$ μm, $a_0 = 0.36$ nm and $\lambda = 1.1\cdot10^{-16}$ cm^2, thus from Eq. (22) $\rho_g = 1.1\cdot10^{-12}$, which is negligible compared with ρ_d for the above grain size. Calculation of $c_t(T_z)$ was made using $E_f = 101.7$ kJ mol^{-1} [65]. An activation energy for unbound vacancies $E_m = 80$ kJ mol^{-1} was estimated [44] and $\rho_{0t} = \rho_{0m} = 4.3\cdot10^{14}$ s^{-1} was taken [44].

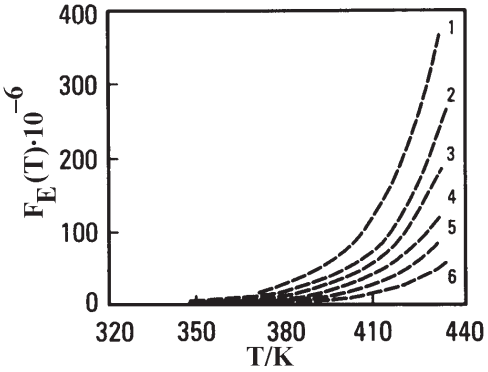

Fig. 5 Function $F_E(T)$ *vs*. temperature for different E values in kJ mol^{-1}; 1 – 80; 2 – 81.9; 3 – 83; 4 – 84.2; 5 – 86 and 6 – 90 kJ mol^{-1}

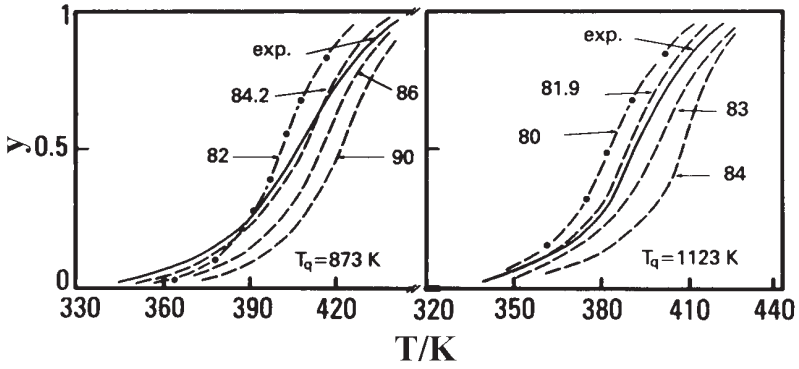

Fig. 6 Experimental and model based reacted fractions, y, during DSC runs at $\phi_r = 0.33$ K s^{-1} in samples quenched from the indicated temperatures for different values of the effective activation energy for defect migration in kJ mol^{-1}

In Fig. 5 the $F_E(T)$ function given by Eq. (31) is plotted against temperature for different values of the effective activation energy for defect migration. As can be seen

$F_E(T)$ is not a function of the quenching temperature and hence of the freezing temperature. Such a function can be easily integrated graphically in the temperature interval 0–T. Figure 6 shows the experimental reacted fractions for T_q= 873 and 1123 K obtained from the corresponding curves as $y = a_t/A$, where a_t is the area under peak to temperature T and A is the total area of the peak. Also calculated y *vs.* T curves are shown for different values of E obtained from Eq. (30). It can be observed that the best fit is different for both quenching temperatures, reflecting the relative importance of unbound and bound vacancies as a function of temperature. Values of E as related to the quenching temperatures were plotted in Fig. 7, but instead of T_q, $c_t(T_z)$ values were employed for convenience as shown later on. It can be noticed that E values slightly decrease with increasing T_z which is a consequence of the lower relative concentration of bound vacancies at higher T_q values.

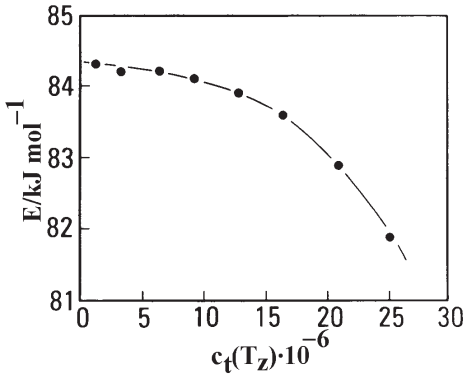

Fig. 7 Effective activation energy E as a function of total defect concentration at freezing temperatures

Activation energy for migration of bound vacancies E_c is obtained from the function $F_c(T)$ shown in Fig. 8, which can be readily integrated graphically in the temperature range 0–T similarly to F_e, and the best fitted y *vs.* T curves to the experimental ones obtained from the corresponding curves. These y *vs.* T curves are shown for T_q= 873 and 1123 K in Fig. 9. If such curves are plotted for other quenching temperatures it is verified that E_c is relative insensitive to T_q. An average of

$$E_c = 89.5\pm0.32 \text{ kJ mol}^{-1}$$

was obtained from four best adjusted values to experimental y *vs.* T curves. Alternative treatments for obtaining E_c were recently given [66, 67].

Defect decay curves can be evaluated from the already known values of E. These curves are shown for T_q= 873 and 1123 K in Fig. 10. The concentration c_u and c_b fall down to zero in pseudo-equilibrium during the DSC scan. Initial boundary values were obtained from the corresponding $c_t(T_z)$ values calculated from Eq. (7) and also from Eqs (9) and (10). Such results are consistent with the one stage ordering shown in the curves of Fig. 1, that is the ordering process is established only by excess defects.

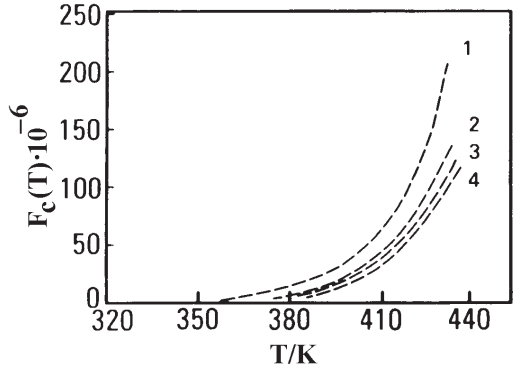

Fig. 8 Function $F_c(T)$ *vs*. temperature for different E_c values. 1 – 80; 2 – 85; 3 – 89.5 and 4 – 95 kJ mol^{-1}

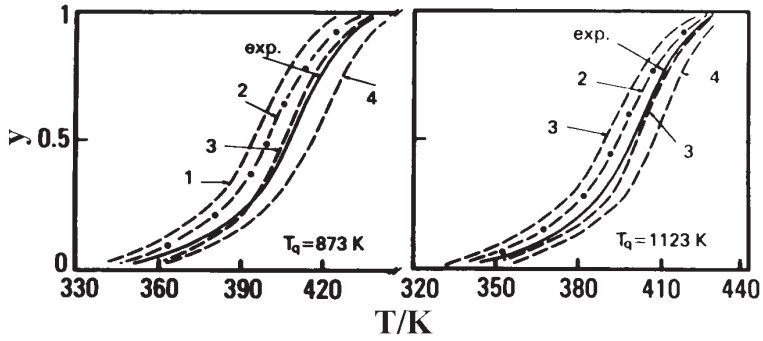

Fig. 9 Experimental and model based reacted fractions, *y*, during DSC runs at ϕ_r=0.33 K s^{-1} in samples quenched from the indicated temperatures for the same values of E_c as those of Fig. 8

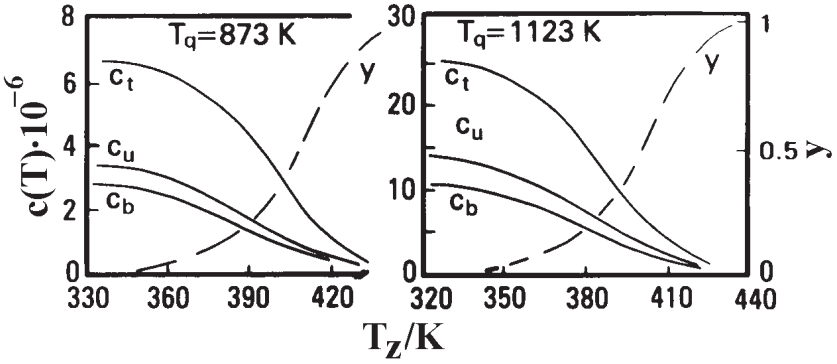

Fig. 10 Bound, unbound and total vacancy concentration decay curves during DSC runs at ϕ_r=0.33 K s^{-1} after quenching from the indicated temperatures. The experimental SRO reacted fractions *y* are also shown

It is worth recalling that even if SRO effects are not larger in this diluted alloy, the heat evolved during DSC runs should correspond to the return of SRO. If one supposes as a first approximation that the heat measured in the curve for an alloy quenched from 973 K, which is about 52 J mol^{-1} (Fig. 1), would correspond to the annealing of quenched-in vacancies, by taking an effective energy of formation of vacancies roughly as E_f–$B/2$ = 91.8 kJ mol^{-1} a quenched-in vacancy concentration extremely high of $5.6 \cdot 10^{-4}$ is calculated, which results are unrealistic for that quench temperature. So, the exothermic peaks observed would be associated unequivocally with SRO. The main reason for employing a diluted alloy within the scope of the present work is that the equilibrium equation between c_u and c_b has restrictions in its use in concentrated alloys, thus turning less rigorous the kinetic analysis.

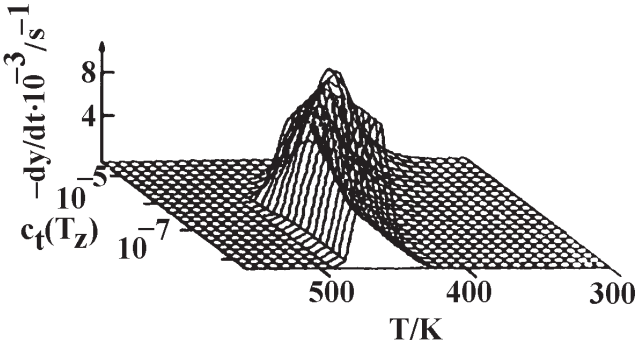

Fig. 11 Generated DSC curves for Cu-5 at% Zn with different initial total defects concentration at freezing temperatures. Heating rate ϕ_r=0.33 K s^{-1}

Finally, in order to get a global insight of the role of the different variables governing the curve profiles, simulated DSC traces (dy/dt)–T–$c_t(T_z)$ are shown in Fig. 11 using the functional dependence of E with $c_t(T_z)$, which appears graphically in Fig. 7. Peak temperatures in Fig. 11 are in very good agreement with those measured in the curves of Fig. 1.

Conclusions

This study leads to the conclusion that the relative importance of solute-vacancy complexes can be quantified by a simple modified first kinetic law model which predicts defect decay concentrations in conjunction with ordering kinetics of quenched alloys during non-isothermal experiments. Comparison of the model based kinetic paths with the experimental ones shows good consistency in Cu–5 at%Zn. Also from ordering kinetic evaluations, the effective activation energy for defect migration and the activation energy for migration of bound vacancies were determined giving quite reasonable values. The relative contribution of bound vacancies to the SRO process becomes more important when quenching temperature decreases as assessed theoretically and observed experimentally. Generated DSC profiles give good concordance with the experimental DSC traces obtained for this alloy.

The authors would like to acknowledge the Fondo de Desarrollo Científico y Tecnológico (FONDECYT) for financial support, Project 1980731 and the Instituto de Investigaciones y Ensayes de Materiales, Facultad de Ciencias Físicas y Matemáticas, Universidad de Chile, for the facilities provided for this research.

References

1 B. Borie and C. J. Sparks. Jr., Acta Crystallogr., 17 (1964) 827.
2 V. I. Iveronova, A. A. Katnslelson and G. P. Revkevich, Fiz. Met. Metalloved., 26 (1968) 106.
3 R. O. Scattergood, S. C. Moss and M. B. Bever, Acta Metall., 18 (1970) 1087.
4 N. Kuwano, Y. Tomokiyo, C. Kinoshita and T. Eguchi, Trans. Jpn. Inst. Met., 15 (1974) 338.
5 Y. Kitano and Y. Kimura, J. Phys. Soc. Jpn., 32 (1972) 1430.
6 J. E. Epperson, P. Furnrohr and C. Ortiz, Acta Crystallogr., A34 (1978) 667.
7 R. W. Cahn and R. G. Davies, Philos. Mag., 5 (1960) 1119.
8 W. Gaudig and H. Warlimong, Z. Metallkd., 60 (1969) 488.
9 Y. Tomokiyo, N. Kuwano and T. Eguchi, J. Phys. Soc. Jpn., 35 (1973) 618.
10 Y. Tomokiyo, K. Kabu and T. Eguchi, Jpn. Inst. Met., 15 (1974) 39.
11 A. Varschavsky, M. I. Pérez and T. Löbel, Metall. Trans., 6A (1975) 577.
12 W. Gaudig and H. Warlimont, Acta Metall., 26 (1978) 709.
13 J. M. Popplewell and J. Crane, Metall. Trans., 2 (1971) 341.
14 C. Kinoshita, T. Tomokiyo, H. Matsuda and T. Eguchi, Trans. Jpn. Inst. Met., 14 (1973) 91.
15 M. Zehetbauer, L. Trieb and H. P. Aubauer, Z. Metallkd., 26 (1976) 431.
16 A. Varschavsky, Mater. Sci. Eng., 22 (1976) 141.
17 A. Varschavsky and E. Donoso, Mater. Sci. Eng., 32 (1978) 65.
18 E. Donoso and A. Varschavsky, Mater. Sci. Eng., 37 (1979) 151.
19 A. Varschavsky and E. Donoso, Mater. Sci. Eng., 40 (1979) 119.
20 A. Varschavsky and E. Donoso, Mater. Sci. Eng. A, 10 (1988) 231.
21 A. Varschavsky and E. Donoso, Mater. Sci. Eng. A, 104 (1988) 141.
22 G. Veith, L. Trieb, W. Puschl and H. P. Aubauer, Phys. Stat. Sol., 27 (1975) 59; Scr. Metall., 9 (1975) 737.
23 A. Varschavsky and E. Donoso, Thermochim. Acta, 69 (1983) 341.
24 M. J. S. Wechsler and R. H. Kernohan, Acta Metall., 7 (1959) 599.
25 L. Trieb and G. Veith, Acta Metall., 26 (1978) 185.
26 C. R. Brooks and E. E. Stansbury, Acta Metall., 11 (1963) 1303.
27 Y. Tomokiyo, N. Kuwano and T. Eguchi, Trans. Jpn. Inst. Met., 26 (1975) 489.
28 A. Varschavsky, Metall. Trans., 13A (1982) 801.
29 A. Varschavsky and E. Donoso, Metall. Trans., 14A (1983) 875.
30 A. Varschavsky and E. Donoso, Metall. Trans., 15A (1984) 1999.
31 A. Varschavsky and E. Donoso, J. Mater. Sci., 21 (1986) 3873.
32 W. Pfeiler, P. Meisterle and M. Zehetbauer, Acta Metall., 32 (1984) 1053.
33 W. Pfeiler, R. Reihsner and D. Trattner, Scr. Metall., 19 (1985) 199.
34 M. Migschitz, F. Laugmayr and W. Pfeiler, Mater. Sci. Eng. A, 177 (1994) 217.
35 M. Migschitz, W. Garlipp and W. Pfeiler, Mater. Sci. Eng. A, 214 (1996) 17.
36 T. Doppler and W. Pfeiler, Phys. Stat. Sol. (a), 131 (1992) 131.
37 M. Spanl, P. Rosenkranz and W. Pfeiler, Mater. Sci. Eng. A, 234 (1997) 541.

38 M. Migschitz, A. Korner, W. Garlipp and W. Pfeiler, Acta Metall. Mater., 44 (1996) 1359.
39 W. Garlipp, M. Migschitz and W. Pfeiler, in Solid–Solid Phase Transformations, Ed. by W. C. Johnson, J. M. Howe, D. E. Laughlin and W. A. Soffa, The Minerals, Metals and Materials Society, 1994, p. 461.
40 M. Migschitz and W. Pfeiler, Mater. Sci. Eng. A, 206 (1996) 155.
41 A. Varschavsky and E. Donoso, Mater. Sci. Eng. A, 145 (1991) 95.
42 A. Varschavsky, Thermochim. Acta, 203 (1992) 391.
43 A. Varschavsky and M. Pilleux, Mater. Letts., 17 (1993) 364.
44 E. Donoso and A. Varschavsky, J. Thermal Anal., 45 (1995) 1419.
45 A. Varschavsky and E. Donoso, Mater. Sci. Eng. A, 212 (1996) 265.
46 J. Plessing, Ch. Achmus, H. Neuhäuser, B. Schönfeld and G. Kostorz, Z. Metallkd., 88 (1997) 630.
47 B. Fultz in, Kinetics of Ordering Transformations in Metals, Ed. by J. Chen and V. K. Vasudevan, The Minerals, Metals and Materials Society, 1992, p. 121.
48 C. R. S. Beatrice, W. Garlipp, M. Cilense and A. T. Adorno, Scr. Metall. Materiallia, 32 (1995) 23.
49 L. S. Chang, E. Rabkin, B. Baretsky and W. Gust, Scr. Materiallia, 38 (1998) 1033.
50 T. Kasuya and M. Fuji, J. Appl. Phys., 83 (1998) 3039.
51 J. Baker, C. J. Girard and C. A. Sholl, Philos. Mag. A, 74 (1996) 543.
52 J. Wolf, M. Franz, J. E. Kluin and D. Schmid, Acta Materiallia, 45 (1997) 4759.
53 A. C. Dasmak and G. J. Dienes, Phys. Rev., 120 (1960) 99.
54 F. Cattaneo and E. Germagnoli, Phys. Rev., 124 (1961) 414.
55 M. Doyama, Phys. Rev., 148 (1966) 683.
56 N. K. Srinivasan and V. Ramachandran, Phys. Stat. Sol., 36 (1969) 673.
57 M. Doyama, Mater. Chem. Phys., 50 (1997) 106.
58 A. C. Dasmask and E. J. Dienes, Acta Metall., 12 (1964) 797.
59 D. V. Ragone, Thermodynamics of Materials, Vol. 2, Wiley, 1995, p. 73.
60 L. K. Mansur, Acta Metall., 29 (1981) 375.
61 M. Halbwachs and J. Hillairet, Phys. Rev., B18 (1978) 4927.
62 C. Sandu and R. Singh, Thermochim. Acta, 159 (1990) 267.
63 E. J. Mittemeijer, J. Mater. Sci., 27 (1992) 3977.
64 A. Borrego and G. Gonzalez-Docel, Mater. Sci. Eng. A., 245 (1998) 10.
65 A. M. Brown and M. F. Ashby, Acta Metall., 28 (1980) 1085.
66 A. Varschavsky and E. Donoso, J. Min. Met., 35B (1999) 255.
67 A. Varschavsky and E. Donoso, Mater. Letts. (in press).